RESEARCH ARTICLE

Eleyon NANOSCALE REPORTS

DOI: 10.26524/nr1831

Synthesis, characterization of visible active MO hallow spheres by combustion technique

G. Thennarasu [a,*], A. Sivasamy [b]

[a] Department of chemistry, C. Kandaswami Naidu College for Men, Unit of pachaiyappa's trust,Chennai-600 102, India.
[b] Chemical Engineering Department, CSIR- Central Leather Research Institute, Adyar,Chennai-600 020, India.

***Corresponding Author**
thennarasuchemistry@gmail.com
(G. Thennarasu)
Tel.: 044 2729 4569

Received : 29-10-2018
Accepted : 21-11-2018

ABSTRACT: A simple method to synthesize nano-sized hallow sphere such as Zn-Ce metal oxide (MO) by combustion technique. The product was characterized by X-ray diffraction (XRD), Field emission-scanning electron microscope (FE-SEM), Fourier transform infrared spectroscopy (FT-IR), Thermo gravimetric analysis (TGA), Diffuse Reflectance Spectroscopy (DRS) and Transmission electron microscope (TEM). The photocatalytic activity of Zn-Ce MO nano-sized hallow sphere was examined by studying the degradation of direct blue 71 (DB71) under visible light irradiations in a slurry photo reactor. The effect of parameters such as the catalyst dosage, concentration of the dye, pH and kinetics on photocatalytic degradation of DB71 is also studied. Degradation of dye was confirmed by UV-VIS spectrum, chemical oxygen demand (COD) and ESI-Mass.

Keywords: Tri azo dye, hallow sphere, visible photocatalyst, combustion technique, degradation

1. Introduction

Visible-light-induced photocatalysts is a prime research area in the field of photocatalysis because of its potential application in clean and renewable energy as well as pollution abatement. The doping of various transition metal cations (V, Cr, Mn, Fe, Co and Ni) [1-5] and anions (N, S, C or B) [6-9] into semiconductors have been extensively studied in order to enhance the activity of photocatalysts under visible-light irradiation. In the case of metal ion doped semiconductors, the doping of metal ion produces impurity states in their forbidden gaps and is responsible for the visible-light absorption [10]. However, the produced impurity states decrease the reduction power of electrons and also act as electron–hole recombination centres, and deteriorate the photocatalytic activity under UV light. In the case of anion-doped semiconductors, even though nitrogen doping can exhibit the visible-light sensitivity, their quantum efficiencies under visible-light are 1–2 orders of magnitude smaller than those under UV light [11-12]. This is due to the oxidation power and mobility of the photo-generated holes in the isolated state, which are lower than those in the valence band (VB) of semiconductors [11, 13]. Therefore, efforts have been focused on designing novel photocatalysts that utilize the high oxidation power of holes under visible-light irradiation.

Cerium oxide is a metal oxides semiconductor which has attracted much interest recently. This is probably because CeO_2 is a semiconductor light absorption in the UV ($\lambda \geq 388nm$) and visible region. Similarly to TiO_2, CeO_2 represents one of the efficient photocatalysts with band gap energy of 3.2eV [14]. Various applications of CeO2 and metal-doped CeO2 include ceramic materials, solid oxide fuel cells, florescent materials, oxygen gas sensors, photoelectrode and catalysts for photocatalytic degradation of organic water pollutants, due to several reasons such as high refractive index, high optical transparency in the visible region, high capacity to store oxygen, strength and agility to react [15-23]. An enhanced photocatalytic activity of CeO_2 can be achieved by doping with transition metal ions such as iron in order to reduce the band gap energy level to be suitable for use in visible light region [24-29]. Photocatalytic process occurring on heterogeneous CeO_2 and Fe doped CeO_2 catalyst is initiated by irradiation from the light source at the appropriate wavelength, which depends on band gap energy of the semiconductor. Many techniques have been proposed for the synthesis of pure CeO_2 and Fe doped CeO_2 such as hydrothermal, spray pyrolysis, sol-gel, gas condensation, sonochemical synthesis and precipitation method [30-35].

In the present study, we used a zinc oxide (ZnO) photocatalyst as a study model, because it is a wide-band-gap semiconductor and has a long history in tuning its electric structure through band-gap narrowing or band-gap widening by the incorporation of various metal ions [36-37]. In this study, we have chosen cerium as the metal incorporated with ZnO, because Ce ions create an impurity state below the CB edge of semiconductors [38]. Although the cerium doped TiO_2 or CeO_2/TiO_2 composites have been reported in the literatures, our strategically way (modification of ZnO with Ce) is the new approach to develop an efficient visible light sensitive photocatalyst [39]. In addition, the reaction kinetics, pH-dependent photocatalytic experiments, and possible photo degradation mechanism in a Zn-Ce MO suspension were also discussed.

2. Experimental

2. 1. Materials and methods

Zinc nitrate hexahydrate (Zn (NO3)2.6H2O), Cerium (III) nitrate hexahydrate (CeN3O9.6H2O) were Sigma-Aldrich, Urea obtained from Merck chemicals, Sodium hydroxide (NaOH) was obtained from Sisco Research Laboratories Pvt. Ltd and hydrochloric acid (HCl) was procured from Ranbaxy Fine Chemicals Ltd and Direct Blue 71 dye (DB71; CAS No: 4399-55-7; molecular weight = 1029.88 g/mol) were S. D. Fine Chemicals Ltd.

The XRD patterns of Zn-Ce MO hallow sphere were obtained using an X' per PRO diffractometer. The morphology of hallow sphere was examined using HITACHI-SU6600 field emission scanning electron microscope (FE-SEM and Transmission electron microscope (TEM) was recorded using Tecnai 10 (Philips model) transmission electron microscope. FT-IR spectra were recorded using Perkin Elmer 6X analyzer in the range 400-4000 cm^{-1} as KBr pellet. The absorption spectra were recorded using a UV-visible spectrophotometer (UV-2101PC). Thermo gravimetric analysis (TGA) of the as-prepared powders were carried out using a thermal analyser (TGA Q50 modal), with a heating rate of 50C min-1 from room temperature to 8000C. The formation of intermediates during the degradation of the dye was monitored by ESI-Mass spectrometer-LCQ Advantage MAX, Thermo Finnigan.

2. 2. Preparation of catalyst

In the combustion method, the metal nitrates (Zn $(NO_3)_2.6H_2O$, $CeN_3O_9.6H_2O$) were dissolved with the fuel (urea) in distilled water and heated (under stirring) on a hot plate at 150°C, until the water evaporation and formation of a gel. After that, the gel was introduced in a muffle furnace, previously heated at 400°C for 1h. Once ignited, the gel underwent a combustion process and yielded a voluminous powder. The powder was than calcined at 500, 700, 900°C for 10h. Finally the powder was in hallowing sphere shape confirmed by FE-SEM analysis. The stoichiometric amount of the propellant was determined by calculation based on the valencies of oxidizing and reducing elements, as determined by the propellant chemistry [40]. The propellant was used in twice the stiochiometric amount.

2. 3. Photocatalytic experiments

Photocatalytic activity studies of the prepared Zn-Ce MO hallow sphere were evaluated by the degradation of DB71 solution using slurry photo reactor as shown in Figure 1(Supplementary material). A 500 W tungsten lamp was used as light source. Prior to each test, the lamp was turned on and warm up for about 30 min in order to get a constant output. Batch tests were performed as the following procedure, 0.6g Zn-Ce metal oxide photocatalyst was added into 200 mL of 0.01g L−1 DB71 solution, the mixture was stirred in dark for 30 min to allow the physical absorption of dye molecules on catalyst to reach the equilibrium. The temperature of the reactions was controlled at room temperature by circulating water. Samples were collected at regular intervals and were immediately filtered and the concentration of DB71 was determined by measuring the absorption intensity at its maximum absorbance wavelength of DB71 by using a UV-Vis spectrophotometer with a 1 cm path length spectrometric quartz cell, and then calculated from calibration curve. The degradation percentage of the dyes wastewaters was obtained by Eq. 1:

$$PDP = [DB71]0-[DB71]/[DB71]*100 \quad (1)$$

where PDP is the abbreviation of the photocatalytic degradation percentage, [DB71]0 is the initial dye concentration, [DB71] is the concentration of dye after visible irradiation.

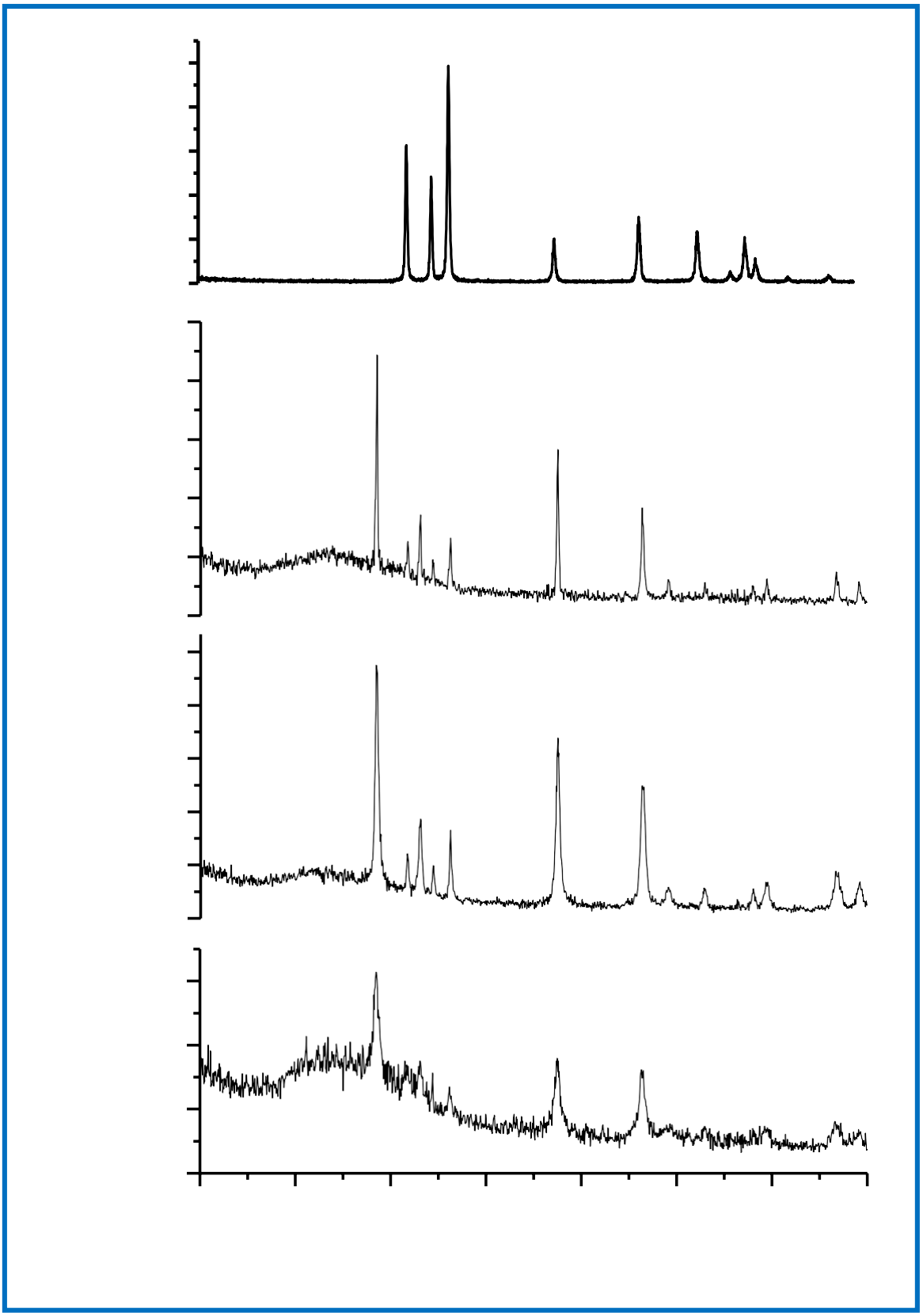

Figure 1. XRD for synthesized ZnO and Zn-Ce MO.

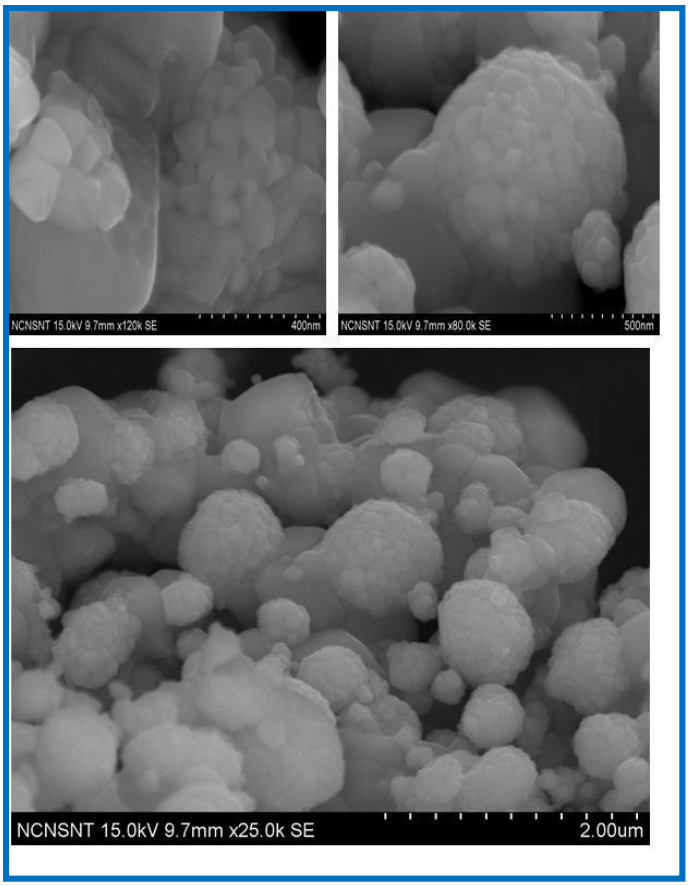

Figure 2. FE-SEM images for synthesized Zn-Ce MO at 900°C-10h

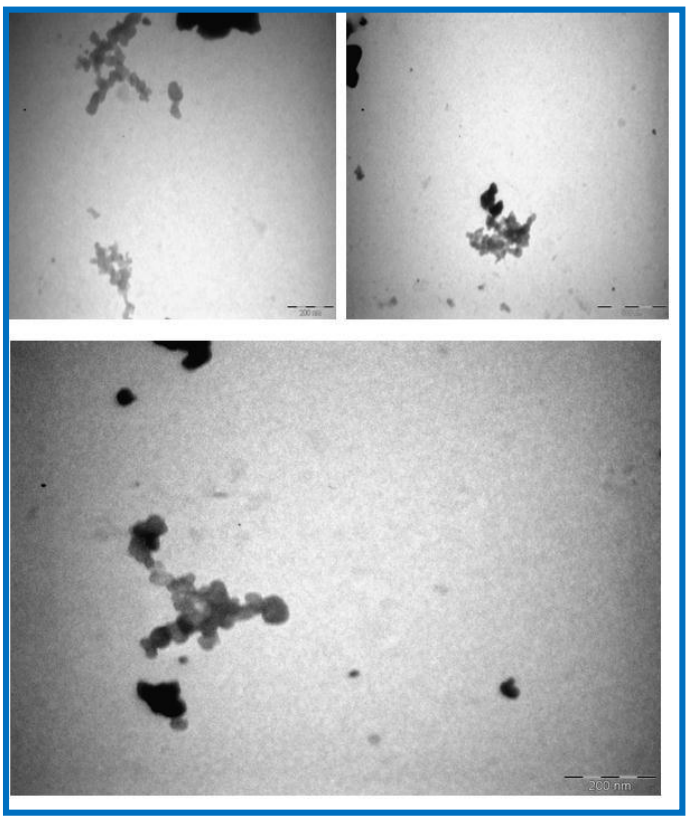

Figure 3. TEM images for synthesized Zn-Ce MO at 900°C-10h.

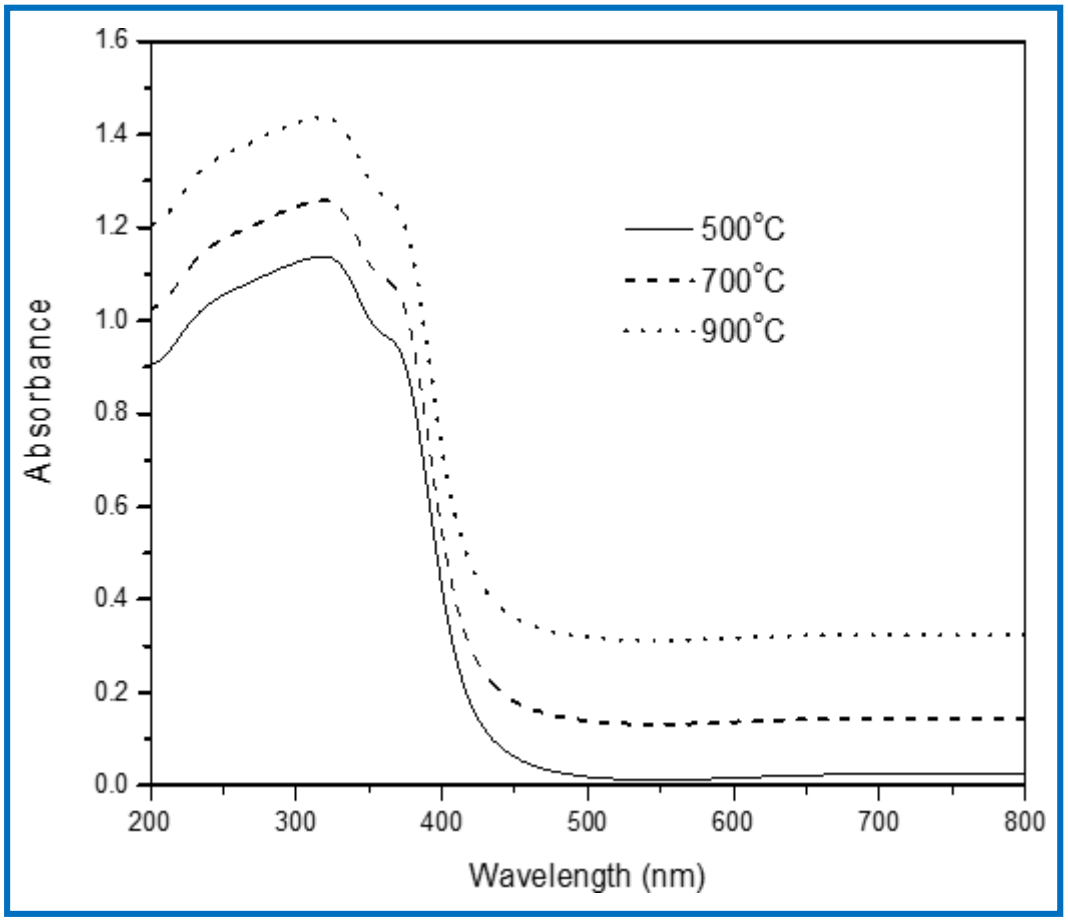

Figure 4. Diffuse reflectance spectra (DRS) for synthesized Zn-Ce MO.

2. 4. Adsorption studies

An adsorption phenomenon is playing an important role in the photocatalytic degradation of pollutants in the aqueous phase. The adsorbed dye on the surface of the photo catalysts acts as an electron donor and further injecting electrons from its excited state to the conduction band of the catalyst under visible irradiation. Adsorption equilibrium experiments were carried out by taking the required amount of catalyst dosage (3 g/ L-1), varying the initial dye concentrations from 0.001 to 0.2 g L-1 and agitating the solutions for 24 h at 100 rpm at 27°C in the dark. The absorbance of the DB71 at 587 nm was measured to determine the equilibrium concentration. The amount of adsorbed dye per gram of Zn-Ce MO at equilibrium concentration, qe (in milligrams per gram), was obtained by Eq. 2:

$$qe=(Co-Ce)V/W \quad (2)$$

Where C0 and Ce (in milligrams per litre) are the initial and equilibrium concentrations of DB 71, respectively, V (in litres) is the volume of the solution and W (in grams) is the weight of catalyst used.

3. Results and discussion

3. 1. Characterization of photocatalyst

Figure 1 shows XRD of as-prepared and calcined (at 500, 700, 900°C for 10 h) Zn-Ce MO samples. Scherrer equation d= 0.94 λ / β cos θ was used to calculate the average crystallite size (8 nm (500°C), 8-18 nm (700°C), 46-74 nm (900°C) for Zn-Ce MO) of the calcined sample. λ denotes the wavelength of the radiation equal to 0.154 nm, β is the full width at half maximum (FWHM) and θ is the half diffraction angle. Figure 1 indicates that the size of the particles increased at increasing calcinations temperature. Further degradation experiments were carried out at 900°C of Zn-Ce MO.

The morphology of the samples was studied by Field emission-scanning electron microscopy. FE-SEM images of Zn-Ce MO samples are calcined at 900°C as shown in Figure 2. The FE-SEM images reveal that, the particle is hallowing sphere shape in the range 40-70 nm for Zn-Ce MO. The FE-SEM micrographs show the voids in the compound, which can be attributed to the large amount of gases escaping out the reaction mixture during combustion.

In combustion synthesis method, it is well known that the morphological characteristics of the product obtained the decomposition, Large volume of gases escaping out facilitate the formation of sphere while the heat released is an important factor for hallow sphere formation. Energy dispersive analysis of X-rays (EDAX) indicates all elements are present within a matrix as shown in Figure 2 (Supplementary material).

Figure 3 displays the TEM micrograph of Zn-Ce MO at 900°C for 10 h. We find that the hallow sphere size of Zn-Ce MO is about 30-50 nm.

The diffuse reflectance spectra of Zn-Ce MO calcined at 500, 700 and 900°C for 10h are displayed in Figure 4. The band-gap energy E_{bg} of the Zn-Ce MO was calculated using the following Eq. 3:

$$Ebg = 1240/\lambda \text{ eV} \quad (3)$$

Where, λ is the wavelength in nano meters. From the above equation we can calculate the band-gab energy Ebg 2.96 (500°C), 2.91 (700°C), 2.88 (900°C) of Zn-Ce MO.

From the above results we can concluded that the Zn-Ce MO is a good visible light active photocatalyst because the absorbance in a visible region.

Figure 3 (Supplementary material) shows TGA curves of the as-synthesized Zn-Ce MO. Thermal decomposition takes place in three stages and burn out of organics is complete at about 700-800°C for Zn-Ce MO. The first decomposition stage, at about 200°C, can be assigned to the loss of adsorbed water; the second, at about 300-600°C, can be associated with the decomposition of combustion residues, mainly fuel that was not burned during fast combustion reactions; and the third, at above 700°C, may be due to complete dissociation of carbonates produced during combustion and initiation of the formation of Zn-Ce MO. The total weight loss of the sample prepared with urea is 0.7% for Zn-Ce MO.

FT-IR spectroscopy was performed to gain more information of the structure and composition of calcined powders. Figure 5 shows the FT-IR spectrum of the synthesized Zn-Ce MO for different temperature and after visible irradiation of DB71. The absorption band at around 1450-1740 cm^{-1} in the as prepared material may be assigned to the unreacted metallic salts and carbonyl (from urea). It shows characteristic Zn-O, O-Ce-O stretching frequencies at 560 cm^{-1}, 717 cm^{-1} and 855 cm^{-1} respectively [41]. FT-IR shows after visible irradiation there is no dye adsorbed on the surface of the catalyst.

3. 2. Characterization of photocatalyst

It is well known that light absorption by photocatalysts and migration of light induced electrons and holes are the most key factors for controlling photocatalytic reaction. When the photocatalyst is exposed to visible light, electrons are excited to the conduction band from the valence band and hence creating holes in the valence band.

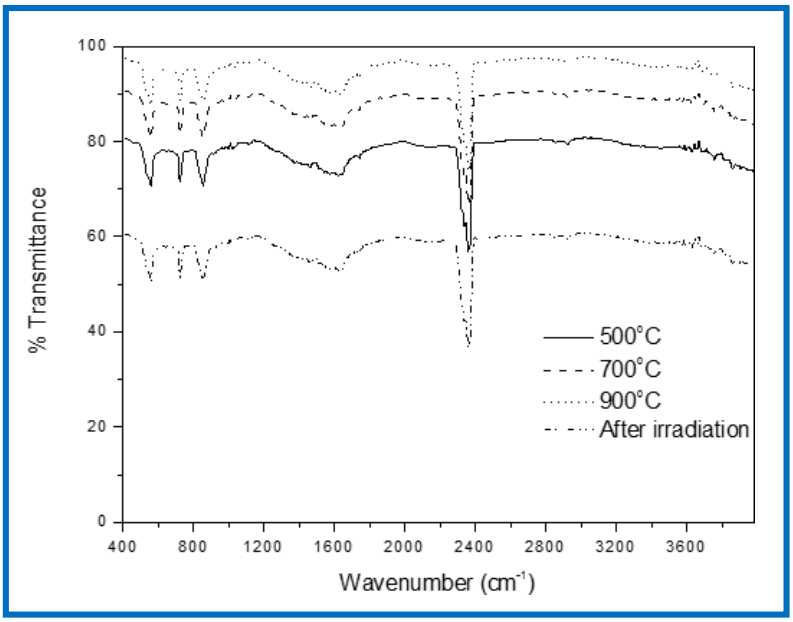

Figure. 5. FT-IR for synthesized Zn-Ce MO and after visible irradiation of DB71

The photo generated hole interacts with the surface hydroxyl group present on the surface of the catalyst to generate the hydroxyl radicals and the photo generated electrons in the conduction band react with the dissolved oxygen forming superoxide radicals which again intermingle with H+ yielding the hydroperoxyl radical followed by the formation of hydrogen peroxide. Then hydroxyl radicals are produced by the attack of photo generated electrons to the hydrogen peroxide.

Throughout this process there is generation of holes, superoxide radicals and hydroxyl radicals which are mostly responsible for photo oxidation of organic pollutants. The mechanisms of formation of these highly active species over the Zn-Ce MO photocatalysts under visible light irradiation are as follows.

$$\text{Zn-Ce MO} + h\upsilon \rightarrow \text{Zn-Ce MO}^* + e^- + h^+ \quad (4)$$

$$h^+ + OH^- \rightarrow OH\bullet \quad (5)$$

$$e^- + O_2 \rightarrow \bullet O_2^- \quad (6)$$

$$\bullet O_2^- + H^+ \rightarrow HO_2\bullet \quad (7)$$

$$HO_2\bullet + HO_2\bullet \rightarrow H_2O_2 + O_2 \quad (8)$$

$$H_2O_2 + e^- \rightarrow OH\bullet + OH^- \quad (9)$$

The formation of hydroxyl radicals, superoxide radicals and holes are mostly responsible for degradation of organic pollutants [42].

3. 3. Role of pH

pH is one of the factors influencing the rate of degradation of some organic compounds in the photocatalytic process [43]. In wastewater treatments, it is also an important operational parameter. Fig. 6a demonstrates the photocatalytic degradation of DB71 at different pH values. The degradation efficiency does not change too much at pH values between 4.3 and 8.6, but the degradation at pH value of 1.8 is significantly lower than those appropriate values. Our observations show that the dye finds low solubility in water at this pH.

The reason for the higher degradation efficiency at pH value of 4.3 is high formation of OH• radicals in acidic solution, as it can be inferred from the above equations (Eq. 5-9) [44].

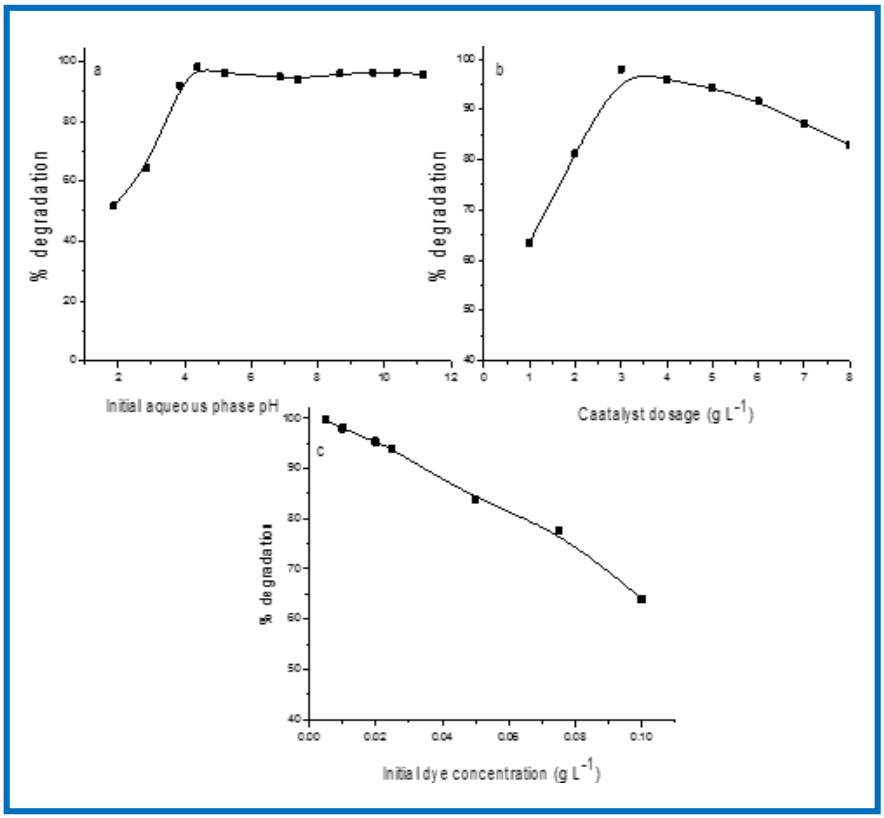

Figure.6. a) Effect of pH; catalyst dosage = 3 g L-1, DB71 = 0.01g L-1 **b)** Catalyst dosage; pH 6.86, DB71 = 0.01gL-**1 c)** Initial DB71 concentration; catalyst dosage = 3 g L-1, pH 6.86

3. 4. Role of pH

In order to optimize the dose of catalyst the experiments were performed by varying catalyst concentration from 1 to 8 g L^{-1} in 0.01g L^{-1} DB71 solutions. The graph plotted (Figure 6b) between amount of catalyst used and percentage degradation reveals that with an increase in catalyst dose degradation efficiency (98%) increases up to 3 g L^{-1} catalyst dose. Due to an increase in turbidity of the suspension with high dose of photocatalyst, there will be decrease in penetration of visible light and hence photoactivated volume of suspension decreases [45]. Moreover, Zn-Ce MO which increases the radiation scattering results in reducing the number of photons absorbed within the reaction space of photocatalytic reactor hence further increase in catalyst dose decreases the degradation efficiency. From the above experiments the optimum dosage of Zn-Ce MO for 0.01g L^{-1} of DB71 solution is 3 g L^{-1}.

3. 5. Effect of the concentration of DB 71

After optimizing the experimental conditions (catalyst dose: 3 g L^{-1}, pH 6.86, time: 90min), the photocatalytic degradation of DB71 was carried out by varying the initial concentrations of the DB71 from 0.005 to 0.1g L^{-1} as shown in Figure 6c. Initial concentration of DB71 increased the degradation percentage decreased due to the path length of the photons entering the solution decreased and increased the number of photons absorbed by the catalyst.

3. 6. Kinetic study

The kinetics of photodegradation of varies concentrations of DB71 using Zn-Ce MO under visible irradiation is demonstrated in Figure 7a. According to previous studies, the influence of initial dye concentration on photocatalytic degradation is described by the Langmuir–Hinshelwood kinetic model [46] which is commonly expressed as

$$-\frac{dc}{dt} = \text{kKC}/(1+KC) \qquad (10)$$

Where k is the reaction rate constant (mg L^{-1} min^{-1}); K is the adsorption coefficient of the reactant (L mg^{-1}); and C is the reactant concentration (mg L^{-1}). When C is very small, KC is negligible with respect to unity and photocatalysis can be simplified to an apparent pseudo-first-order kinetics.

$$-\frac{dc}{dt} = k\text{KC} \qquad (11)$$

$$In\frac{Co}{Ce} = kKC = K_{app}\,t \qquad (12)$$

Where kapp. is the apparent pseudo-first-order rate constant (min−1).

The linear fit between ln(Co/Ce) and irradiation time (t) under different initial DB71 concentrations can be used to describe the pseudo-first-order kinetics. Results are shown in Fig. 7b. All correlation coefficients were higher than 0.999, indicating that the proposed kinetic model was in good agreement with our experimental data. The order of rate constants and half life t½ (minutes) i.e., t½ = 0.693/k for all the above experiments is given Table 1. Therefore, the initial dye concentration had a fundamental effect on the degradation rate, i.e., the rate constant decreased with the increase in initial DB71 concentration.

Table 1 Pseudo first order rate constants of visible photo degradation of DB71

Initial Dye concentration (g L^{-1})	0.01	0.025	0.05	0.075
Kobs (min-1)	0.0651	0.0467	0.0304	0.0177
t ½	10.64	14.83	22.79	39.15

3. 7. Adsorption isotherms

Sorption of the dye is an important parameter in determining photocatalytic degradation rate. Adsorption tests in the dark were carried out in order to evaluate the equilibrium constants of the adsorption of the dye on the photocatalyst surface. The Langmuir and Freundlich isotherms were employed to determine the adsorption isotherm parameters, which were obtained by plots of 1/qe versus 1/Ce. The results are shown in Figure 7(c & d). The theoretical Langmuir isotherm is based on the assumption that adsorption occurs at specific homogeneous sites within the catalyst and the capacity of the catalyst is finite. Langmuir equation (Eq.13) is represented as follows:

$$q_q = \frac{kK_L C_e}{1 + q_m C_e}$$

where Ce is the equilibrium concentration (in milligrams per litre), q_e is the amount of dye adsorbed at equilibrium (in milligrams per gram), qm is the maximum adsorption

monolayer saturation capacity of catalyst (in milligrams per gram) for a complete q_e, which gives, and KL is the sorption equilibrium constant (in litres per milligram). The essential features of the Langmuir isotherm can be expressed in terms of a dimensionless constant called separation factor (RL) also called known as the equilibrium parameter which is defined by the following Eq. 14:

$$R_L = \frac{1}{1+K_L C_O} \quad (14)$$

Where C0 (in milligrams per litre) is the initial DB71 concentration and qm (in milligrams per gram) is the Langmuir constant related to the energy of adsorption. The value of RL indicates the shape of the isotherms to be either unfavourable (RL>1), linear (RL=1), favourable (0<RL<1) or an irreversible (RL=0). isotherm plot is shown in Figure 7c, and the parameters obtained from this plot are tabulated in Table 2.

The Freundlich isotherm is consistent with exponential distribution of active centres and the characteristics of heterogeneous surfaces on adsorption. The Freundlich isotherm equation (Eq. 15) is expressed as:

$$q_e = KFCC_e 1/n \quad (15)$$

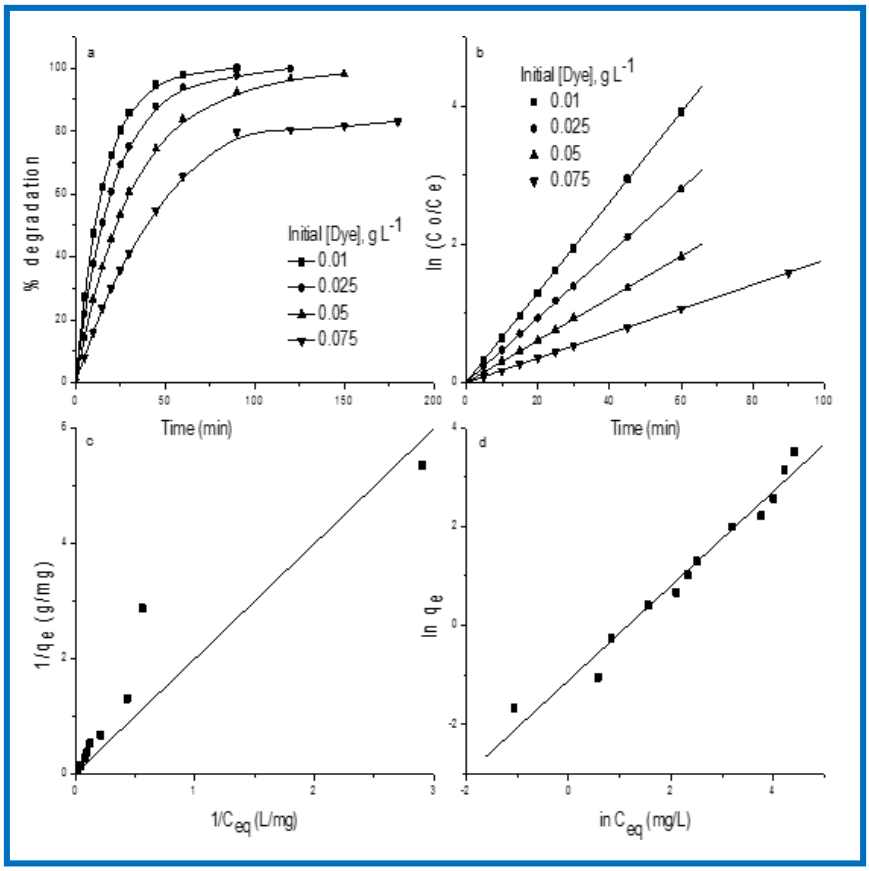

Figure .7. a) Kinetics **b)** Pseudo first order kinetic plot of visible photo degradation of DB71; catalyst dosage = 3 g L-1, DB 71 = 0.01, 0.025, 0 .05, 0.075 g L-1 **c)** Langmuir isotherm **d)** Fruendlich isotherm; catalyst dosage = 3g L-1, pH 6.86, T =27°C; t=24h; agitation =100 rpm

Table 2 The constants of Langmuir and Freundlich isotherms of DB71 by visible light

Isotherms						
Langmuir			Fruendlich			
q_m(mg/g)	K_L	R_L	r^2	K_F (L/g)	N	r^2
3.6363	0.0668	0.0696-0.9373	0.9735	0.1612	0.9623	0.9418

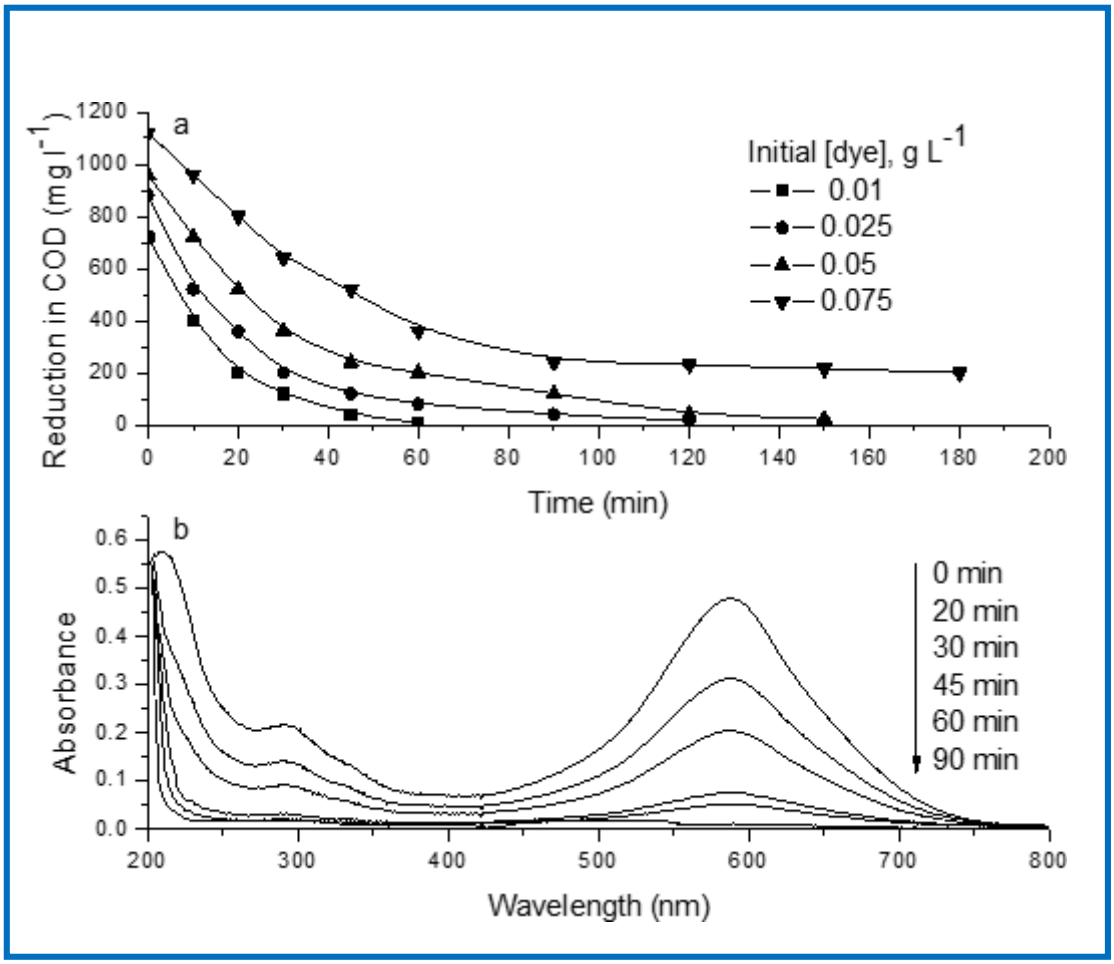

Figure.8. a) Reduction in COD of the DB71solution at various concentrations **b)** Spectral changes of DB71 during visible photo catalytic degradation in the presence of Zn-Ce MO.

Where KF is the binding energy constant reflecting the affinity of the adsorption (in litres per gram) and n is the Freundlich exponent related to adsorption intensity. The Freundlich isotherm plot is shown in Figure 7d, and the parameters obtained from this plot are given in Table 2.

3. 8. Chemical oxygen demand (COD)

The COD is an effective technique to measure the strength of organic content present in wastewater. This test allows the measurement of total quantity of oxygen required for the complete oxidation of organic matter to carbon dioxide and water. Figure 8a indicates the reduction in COD of the DB71 solutions at various concentrations before and after visible irradiation. It could be observed that the reduction observed in COD values of the treated DB71 solution indicated complete mineralization of DB71 molecules along with the removal of colour.

3. 9. UV-VIS absorption spectrum

The UV-Vis absorption spectrum of DB71 consists of two main peaks at 358 and 587 nm. The band at 358 nm arises from the π– π* transition related to the aromatic ring attached to the –N=N– group in the DB71 molecule, whereas the 587 nm band could be assigned to the n– π* transition of the –N=N– group. During the degradation process, it was observed that the two characteristic absorption peaks at 358 and 587 nm decreased and almost disappeared during the course of the study as shown in Figure 8b. This shows that the chromophore and conjugated system were being destroyed. For degradation studies, the λmax of the DB71 (587 nm) was chosen for further investigations.

3. 9. Degradation pathway

Oxidation plays an important role in the detoxification of various hazardous dyes by carrying out oxidative cleavage

[47]. Figure 4 & 5 (supplementary material) shows the ESI-Mass for pure DB71 & after 30 min irradiation of DB71. We have proposed a pathway for degradation of DB71 on the basis of ESI-Mass analysis was already published in previous work [48].

3. 11. Reusability

Recycling use of photocatalyst is very important for the practical application. Studies reported that the photocatalysts would be inactivated by the accumulation of intermediate product around the surface of metal oxide [49-50]. Therefore, its photocatalytic activity is reduced when recycling. In this paper, the effect of run times on the DB71 degradation over photocatalysts was studied. The results are illustrated in Figure 9. It is shown that Zn-Ce MO had higher photocatalytic activity (about 89%) after used third times, which suggested that Zn-Ce MO could reduce the inactivation of photocatalysts and extend the using time. In addition, the analysis of FT-IR also confirmed the chemical stability of catalyst during the three recycles (Figure 5).

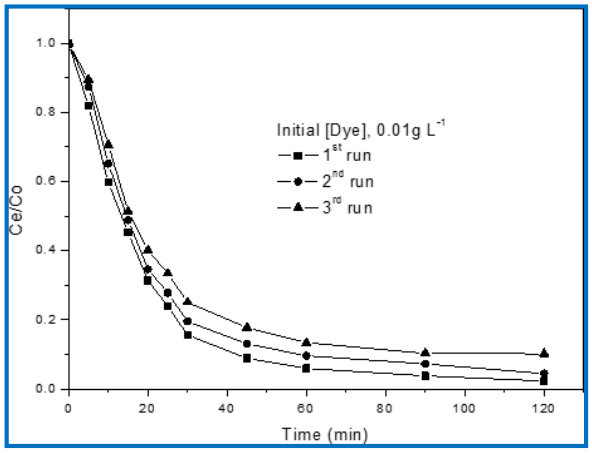

Figure 9. Reusability of the catalyst on the degradation of DB71 for three runs by Zn-Ce MO; DB71= 0.01g L-1, pH 6.86, catalyst dosage = 3 g L-1, irradiation time = 90 min.

4. Conclusion

In summary, we conclude that the present study represents a new strategy for the development of efficient visible light photocatalysts using metal ion incorporated metal oxide semiconductors. The fastest degradation of DB71 occurred under the optimal conditions with 3 g L-1 of Zn-Ce MO hallow sphere, pH 6.86, 0.01g L-1 of DB71 and 90 min visible irradiation. Based on the identification of products by ESI-Mass, the degradation pathways of DB71 were proposed. Moreover, Zn-Ce MO hallows sphere showed excellent reusability in heterogeneous visible light reaction. Adsorption isotherm data well fitted with the Langmuir adsorption equilibrium models. The value of separation factor RL of Langmuir isotherm was well in between 0 and 1 confirming the adsorption process as favourable. The Freundlich constant (n) fell between 1 and 10 indicating that the adsorption process was favourable. The visible photo degradation of DB71 was found to exhibit pseudo first order kinetics.

References

[1] E. Borgarello, J. Kiwi, M. Graetzel, E. Pelizetti and M. Visca, Visible light induced water cleavage in colloidal solutions of chromium-doped titanium dioxide particles, *Journal of the American Chemical Society*, 104 (1982) 2996-3002.

[2] W. Choi, A. Termin and M. R. Hoffmann, The Role of Metal Ion Dopants in Quantum-Sized TiO_2: Correlation between Photoreactivity and Charge Carrier Recombination Dynamics, *The Journal of the Physical Chemistry*, 98 (1994) 13669-13679.

[3] M.A. Henderson, J.M. White, H. Uetsuka and H. Onishi, Photochemical Charge Transfer and Trapping at the Interface between an Organic Adlayer and an Oxide Semiconductor, *Journal of the American Chemical Society*, 125 (2003) 14974-14975.

[4] M. Anpo and M. Takeuchi, Design and development of second-generation titanium oxide photocatalysts to better our environment-approaches in realizing the use of visible light, *International Journal of Photoenergy*, 3 (2001) 89-94.

[5] M. Anpo, M. Takeuchi, The design and development of highly reactive titanium oxide photocatalysts operating under visible light irradiation, *Journal of Catalysis*, 216 (2003) 505-516.

[6] C.W. Dunnill, Z. Ansari, A. Kafizas, S. Perni, D.J. Morgan, M. Wilson, I. P. Parkin, Visible light photocatalysts—N-doped $TiO_2$by sol–gel, enhanced with surface bound silver nanoparticle islands, *Journal of Material Chemistry*, 21 (2011) 11854-11861.

[7] J.M. Herrmann, J. Disdier, P. Pichat, Effect of chromium doping on the electrical and catalytic properties of powder titania under UV and visible illumination, *Chemical Physics Letters*, 108 (1984) 618-622.

[8] E. Borgarello, J. Kiwi,E. Pelizetti, M. Visca and M. Gratzel, Photochemical cleavage of water by photocatalysis, *Nature*, 289 (1981) 158.

[9] I. Nakamura, N. Negishi, S. Kutsuna, T. Ihara, S. Sugihara K. Takeuchi, Role of oxygen vacancy in the plasma-treated TiO2 photocatalyst with visible light activity for NO removal, *Journal of Molecular Catalysis A: Chemical*, 161 (2000) 205-212.

[10] U. Diebold, The surface science of titanium dioxide, *Surface Science Reports*, 48 (2003) 53-229.

[11] H. Irie, Y. Watanabe, K. Hashimoto, Nitrogen-Concentration Dependence on Photocatalytic Activity of TiO2-xNx Powders, Journal of Physical Chemistry *B*, 107 (2003) 5483–5486.

[12] M. Miyauchi, A. Ikezawa, H. Tobimatsu, H. Irie, K. Hashimoto, Zeta potential and photocatalytic activity of nitrogen doped TiO2 thin films, *Physical Chemistry Chemical Physics*, 6 (2004) 865-870.

[13] R. Nakamura, T. Tanaka and Y. Nakato, Mechanism for Visible Light Responses in Anodic Photocurrents at N-Doped TiO2 Film Electrodes, *Journal of Physical Chemistry B*, 108 (2004) 10617–10620.

[14] R.G. Toro, G. Malandrino, L. Fragala, Relationship between the Nanostructures and the Optical Properties of CeO2 Thin Films, *Journal of Physical Chemistry B*, 108 (2004) 16357–16364.

[15] T.S. Zhang, J. Ma, S.H. Chen, J.A. Kilner, Grain boundary conduction of Ce0.9Gd0.1O2−δ ceramics derived from oxalate coprecipitation: effects of Fe loading and sintering temperature, *Solid State Ionics*, 176 (2005) 377-384.

[16] B.G. Pound, Comment on "The characterization of doped CeO_2 electrodes in solid oxide fuel cells, *Solid State Ionics*, 52 (1992) 183–188.

[17] I.A. Siddiquey, T. Furusawa, Y. Hoshi, E. Ukaji, F. Kurayama, M. Sato, N. Suzuki, Silica coating of CeO_2 nanoparticles by a fast microwave irradiation method, *Applied Surface Science*, 255 (2008) 2419-2424.

[18] N. Izu, W. Shin, N. Murayama and S. Kanzaki, Resistive oxygen gas sensors based on CeO_2 fine powder prepared using mist pyrolysis, *Sensors and Actuators B: Chemical*, 87 (2002) 95-98.

[19] P. Ji, J. Zhang, F. Chen and M. Anpo, Study of adsorption acid orange 7 on CeO_2 under visible light irradiation *Applied Catalysis B: Environmental*, 85 (2009) 148-154.

[20] S. Kanakaraju, S. Mohan and A.K. Sood, Optical and structural properties of reactive ion beam sputter deposited CeO_2 films, *Thin Solid Films*, 305 (1997) 191-195.

[21] C.O. Avellaneda, M.A.C. Berton, L.O.S. BulhÕes, Optical and electrochemical properties of CeO2 thin film prepared by an alkoxide route, *Solar Energy Materials and Solar Cells*, 92 (2008) 240-244.

[22] A. Wongkaew, Effect of Cerium Oxide and Zirconium Oxide to Activity of Catalysts, *Chiang Mai Journal of Science*, 35 (2008) 156-162.

[23] H.J. Choi, J. Moon, H.B. Shim, K.S. Han, E. Lee, and K.D. Jung, Preparation of nanocrystalline CeO2 by the precipitation method and its improved methane oxidation activity, *Journal of the American Ceramic Society*, 89 (2006) 343–345.

[24] F. Galindo, R. Gómez, M. Aguilar, Photodegradation of the herbicide 2,4-dichlorophenoxyacetic acid on nanocrystalline TiO2–CeO2 sol–gel catalysts, *Journal of Molecular Catalysis A: Chemical*, 281 (2008) 119-125.

[25] T. Arai, K. Maruya, K. Domen, T. Onishi, Strongly adsorbed species to form linear hydrocarbons over partially reduced CeO2, *Journal of Catalysis*, 141 (1993) 533-539.

[26] A.M.T. Silva, R.R.N. Marques, R.M. Quinta-Ferreira, Catalysts based in cerium oxide for wet oxidation of acrylic acid in the prevention of environmental risks, *Applied Catalysis B: Environmental*, 47 (2004) 269-279.

[27] D.F. Ollis, Photocatalytic purification and remediation of contaminated air and water, *Comptes Rendus De 1'Académie Des Sciences-Series IIC-Chemistry* 3 (2000) 405-411.

[28] K.H. Chung and D.C Park, Water photolysis reaction on cerium oxide photocatalysts, *Catalysis Today*, 30 (1996) 157-162.

[29] J. Belošević-Čavor, V. Koteski, A. Umićević, V. Ivanovski, Effect of 5d transition metals doping on the photocatalytic properties of rutile TiO2, *Computational Materials Science* 151 (2018) 328–337.

[30] T. Masui, H. Hirai, N. Imanaka, G. Adachi, T. Sakata, H. Mori, Synthesis of cerium oxide nanoparticles by hydrothermal crystallization with citric acid, *Journal of Materials Science Letters*, 21 (2002) 489-491.

[31] B. Elidrissi, M. Addou, M. Regragui, C. Monty, A. Bougrine and A. Kachouane, Structural and optical Properties of CeO2 Thin Films Prepared by Spray Pyrolysis, *Thin Solid Films*, 379 (2000) 23-27.

[32] N. Phonthammachaia, M. Rumruangwonga, E. Gularib, A.M. Jamiesonc, S. Jitkarnkaa, S. Wongkasemjita, Colloids and Surfaces A: *Physicochemical and Engineering Aspects*, 247 (2004) 61-68.

[33] N. Guillou, L.C. Nistor, H. Fuess, H. Hahn, Microstructural studies of nanocrystalline CeO2 produced by gas condensation, *Nanostructured Materials*, 8 (1997) 545-557.

[34] L.X. Yin, Y.Q. Wang, G.S. Pang, Y. Koltypin, A. Gedanken, Sonochemical synthesis of cerium oxide nanoparticles-effect of additives and quantum size effect, *Journal of Colloid and Interface Science*, 246 (2002) 78-84.

[35] H.I. Chen, H.Y. Chang, Homogeneous precipitation of cerium dioxide nanoparticles in alcohol/water mixed solvents, *Colloids and Surfaces A: Physicochemical and Engineering Aspects*, 242 (2004) 61-69.

[36] V. Kruefu, E. Peterson, C. Khantha, C. Siriwong, S. Phanichphant, D.L. Carroll, Flame-made niobium doped zinc oxide nanoparticles in bulk heterojunction solar cells, *Applied Physics Letters*, 97 (2010) 053302.

[37] M.K. Yadav, M. Ghosh, R. Biswas, A.K. Raychaudhuri, A. Mookerjee, S. Datta, *Physical Review B*, 76 (2007) 195450.

[38] J.H. Lang, Q. Han, J.H. Yang, C.S. Li, X. Li, L.L. Yang, Y.J. Zhang, M. Gao, D.D. Wang, Fabrication and Optical Properties of Ce-Doped ZnO Nanorods, *Journal of Applied Physics*, (107) 2010, 74302.

[39] G. Li, D. Zhang, J.C. Yu, Thermally stable ordered mesoporous CeO2/TiO2 visible-light photocatalysts, *Physical Chemistry Chemical Physics*, 11 (2009) 3775-3782.

[40] A. Ringuedé, J.A. Labrincha, J.R. Frade, A combustion synthesis method to obtain alternative cermet materials for SOFC anodes, *Solid State Ionics*, 141 (2001) 549-557.

[41] S.R. Kulal, S.R. Bamane, Synthesis of Cerium doped Zinc oxide nanoparticles by aqueous hydrothermal method and study of their properties, *Archives of Applied Science Research*, 2 (2010) 205-210.

[42] S. Ge, L. Zhang, Efficient Visible Light Driven Photocatalytic Removal of RhB and NO with Low Temperature Synthesized In(OH)xSy Hollow Nanocubes: A Comparative Study, *Environmental Science & Technology*, 45 (2011) 3027–3033.

[43] C. Wu, X. Liu, D. Wei, J. Fan, L. Wang, Photosonochemical degradation of phenol in water, *Water Research*, 35 (2001) 3927-33.

[44] Y. Chen, Z. Sun, Y. Yang, Q. Ke, Heterogeneous photocatalytic oxidation of polyvinyl alcohol in water, *Journal of Photochemistry and Photobiology A: Chemistry*, 142 (2001) 85–89.

[45] N. Daneshvar, D. Salari and A.R. Khataee, Photocatalytic degradation of azo dye acid red 14 in water: investigation of the effect of operational parameters, *Journal of Photochemistry and Photobiology A: Chemistry*, 157 (2003) 111-116.

[46] T. Sauer, G.C. Neto, H.J. José, R.F.P.M. Moreira, Kinetics of photocatalytic degradation of reactive dyes in a TiO_2 slurry reactor, *Journal of Photochemistry and Photobiology A: Chemistry*, 149 (2002) 147-154.

[47] U. Jadhav, V. Dawkar, D. Tamboli, S. Govindwar, Purification and characterization of veratryl alcohol oxidase from Comamonas sp. UVS and its role in decolorization of textile dyes, *Biotechnology and Bioprocess Engineering*, 14 (2009) 369.

[48] G. Thennarasu, A. Sivasamy, Enhanced visible photocatalytic activity of cotton ball like nano structured Cu doped ZnO for the degradation of organic pollutant, *Ecotoxicology and Environmental Safety*, 134 (2016) 412- 420.

[49] K.K. Ioannis, A.S. Wasilios, A.A. Triantafyllos, Photocatalytic degrada- tion of the herbicides propanil and molinate over aqueous TiO_2 sus- pensions: identification of intermediates and the reaction pathway, *Applied Catalysis B: Environmental*, 34 (2001) 227-239.

[50] C. L. Li and Y. L. Fu, Effect on the Carbon Deposit in CO_2 Reforming of CH_4 over Ni/Ce-Zr-Al-Ox Catalyst by Adding Steam, *Acta. Physica Chimico Sinica*, 20 (2004) 906-910.

Competing Interests:

The authors declare that they have no competing interests.

About The License